IJARCCE ISSN (O) 2278-1021, ISSN (P) 2319-5940



International Journal of Advanced Research in Computer and Communication Engineering

Impact Factor 8.471 ⁜ Peer-reviewed & Refereed journal ⁜ Vol. 15, Issue 11, November 2026

DOI: 10.17148/IJARCCE.2026.1511139

AWGN Seed-Coded FH-FMCW Radar with 4×4 MIMO Digital Beamforming

Adithi Sreenivas[1], Aneesh P Bhagvat[2], Vasishta R B[3], Dr. Venu Gopal B T[4], Harshwardhan Sharma[5]

Department of Electronics and Communication Engineering, RV Institute of Technology and Management, Bangalore, India[1-5]

Abstract: Radar waveforms built from identical, repeating chirps are easy to intercept and jam. This paper surveys the literature behind an additive white Gaussian noise (AWGN) seed-coded, frequency-hopping FMCW radar with a 4×4 MIMO array and digital beamforming, and describes the hardware planned around it. The survey covers phase-coded and noise-like waveforms, MIMO waveform separation, phase-noise limits, software-defined radio (SDR) platforms, multi-channel beamforming, and the antenna and RF parts needed at X and Ku band. The planned system uses two AD9363 SDR boards in 2×2 mode, an RF distribution board built around an ADF4372 synthesizer, an ADRF5020 switch and a Wilkinson divider, ADAR1000 beamformers, and a front end with a power amplifier, directional coupler, filters and low-noise amplifier. Only antenna-level results exist so far. Simulation at 10 GHz shows a directional main lobe and S11 below −10 dB near resonance, which supports the antenna design but does not yet validate the waveform, the distribution network or the beamformer. The works we reviewed treat these pieces separately, and combining them on one SDR platform is the gap this project targets.

Index Terms: AWGN, FH-FMCW radar, MIMO radar, digital beamforming, hybrid beamforming, software-defined radio, low probability of intercept, X-band, Ku-band, antenna array, RF distribution.

I. INTRODUCTION

Radar measures the range, radial velocity and direction of a target without any help from the target, which is why it is used in surveillance, defence, aerospace and sensing [1], [2].

A conventional FMCW radar sends the same chirp again and again. The spectrum and timing are predictable, so the signal is easier to intercept, interfere with or jam [1], [3].

Phase-coded and noise-like waveforms lower that predictability while keeping the autocorrelation properties that detection depends on [1], [4]–[6]. Frequency hopping adds more variation by moving the carrier between sub-bands, and if the sub-band measurements are combined coherently the effective bandwidth grows. The effect of band-hopping jamming on hopping links has been studied in simulation [7].

MIMO radar uses several transmit and receive elements to build a larger virtual aperture and sharpen angular resolution. The price is that the transmitted waveforms must be close to orthogonal and the phase must stay coherent across every channel [1], [2], [8]. At X and Ku band, phase noise, RF path mismatch, channel coupling, gain imbalance and timing error can all degrade coherent processing badly [9], [10].

This paper surveys work on these topics and uses it to define one system: an AWGN seed-coded FH-FMCW waveform, SDR-based IF generation and acquisition, a phase-coherent RF distribution board, ADAR1000 analog beam steering and a four-transmit, four-receive antenna array [1], [9], [10]. The target RF range is 8–16 GHz, set by the beamformer and front-end parts, and two AD9363 SDR boards generate and acquire the signals.
Section II reviews the literature, Section III gives the system model, Section IV describes the implementation plan, Section V reports the results available so far, and Section VI concludes.

II. LITERATURE SURVEY

A. Waveform Design

Kumbul et al. studied phase-coded FMCW for coherent MIMO radar and showed that the coding lets several transmitters work at once while sidelobes and range resolution stay under control [1]. Their smoothed variant cuts out-of-band spectral

 This work is licensed under a Creative Commons Attribution 4.0 International License

IJARCCE ISSN (O) 2278-1021, ISSN (P) 2319-5940



International Journal of Advanced Research in Computer and Communication Engineering

Impact Factor 8.471 ⁜ Peer-reviewed & Refereed journal ⁜ Vol. 15, Issue 11, November 2026

DOI: 10.17148/IJARCCE.2026.1511139

energy and keeps the basic radar waveform properties [4]. Uysal covered the design of phase-coded FMCW radar and its interference suppression, and argued that waveform diversity matters when other radars share the environment [3]. Noise-radar work shows that noise-like waveforms can be detected with correlation or matched-filter processing, and examines the range–Doppler resolution of a linear-FM noise waveform [5], [6]. The costs are autocorrelation sidelobes and the difficulty of isolating the transmitter from the receiver.

B. MIMO Waveform Separation

Overdevest et al. showed that Doppler shift can destroy the orthogonality between transmitted codes in phase-coded MIMO radar, so a code set that separates well for static targets can fail for moving ones [8]. Park et al. used MIMO FMCW radar for indoor mapping from multipath returns, which shows what multi-channel processing adds for sensing [2].

C. Phase Noise and Hardware Errors

Tschapek et al. showed that oscillator phase noise and systematic phase distortion limit FMCW measurement accuracy. Their results point to stable frequency references and matched RF signal paths [9].

D. SDR and Multi-Channel Platforms

Petri and Ehrig described a SoC-based SDR platform for communication, radar and localization [11], and Grigoriev et al. validated the LibreSDR board [12]. Yang et al. built a 4×4 digital beamforming receive array on synchronized RFSoCs, which shows how much coherent multi-channel work depends on shared clocks and sampling [10]. Yan et al. integrated the digital and microwave parts of an active phased array on one composite board [13].

E. Antennas, Filters and Couplers

Two antipodal Vivaldi designs cover gain improvement in a compact element [14] and multiband operation for non-contact radar sensing [15]. For the receive chain, wideband bandpass filters with very broad stopbands are relevant [16], and a high-directivity coupler design is relevant for sampling transmit power [17].

F. Summary and Research Gap

Table I summarizes the surveyed work and how each item bears on this project.

TABLE I. SUMMARY OF SURVEYED WORK

Ref.	Contribution	Use here
[1]	Phase-coded FMCW for coherent MIMO	Basis for coded transmit channels
[2]	MIMO FMCW mapping from multipath	Value of multi-channel processing
[3]	Interference mitigation by waveform diversity	Motivation for diverse waveforms
[4]	Smoothed coding, low out-of-band energy	Clean spectrum
[5]–[7]	Band-hopping jamming; noise waveforms and processing	Hopping and noise-like waveform basis
[8]	Doppler breaks code orthogonality	Limit on MIMO separation
[9]	Phase noise and phase distortion in FMCW	Common reference, matched paths
[10], [13]	Synchronized 4×4 beamforming array; integrated array board	Channel synchronization and integration
[11], [12]	SoC-based SDR; LibreSDR validation	SDR platform choice
[14], [15]	Compact and multiband Vivaldi antennas	Antenna element choice
[16], [17]	Wideband filters; directional coupler	Receive filtering, power sampling

The waveform papers [1], [3], [4], [8] and the hardware papers [9]–[13] mostly address one block at a time. This project aims to join waveform diversity, coherent frequency distribution, RF switching and conditioning, analog beam steering and multi-channel SDR processing in one working system [1], [9], [10]. The survey leaves three points open: whether the code set still separates under Doppler [8], whether phase coherence holds across all 16 transmit–receive pairs [9], [10], and whether hop-to-hop phase repeatability is good enough to combine sub-bands coherently [7], [9].

III. SYSTEM MODEL

A. System Architecture

The system has three subsystems: an SDR board assembly (Fig. 1), an RF distribution board (Fig. 2) and a transmit/receive front-end module (Fig. 3).

IJARCCE ISSN (O) 2278-1021, ISSN (P) 2319-5940

International Journal of Advanced Research in Computer and Communication Engineering

Impact Factor 8.471 ⁜ Peer-reviewed & Refereed journal ⁜ Vol. 15, Issue 11, November 2026

DOI: 10.17148/IJARCCE.2026.1511139

The SDR assembly holds two AD9363 units, each in 2×2 intermediate-frequency (IF) mode on a Zynq 7020 processing platform [12]. Together they give four transmit and four receive channels, and they are the main signal generation and acquisition interface.

The distribution board routes IF/RF signals and the reference clock between the SDR units, the frequency synthesizer, the conversion and gain stages, the RF switches and the ADAR1000 beamformers.

The front-end module connects the conditioned RF paths to the transmit and receive antennas. It provides transmit power amplification, power monitoring, receive filtering and low-noise amplification [17].

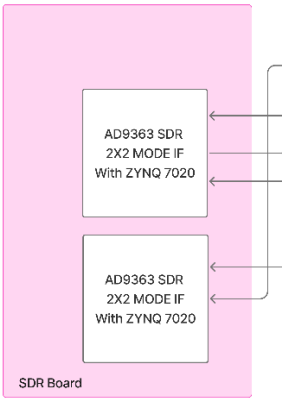


Fig. 1. SDR board.

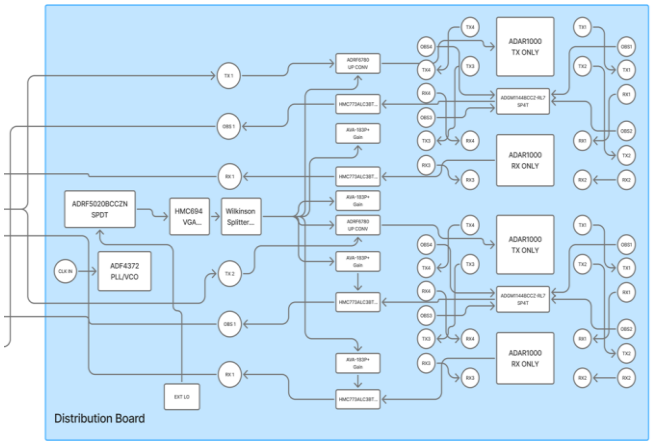


Fig. 2. RF distribution board block diagram.

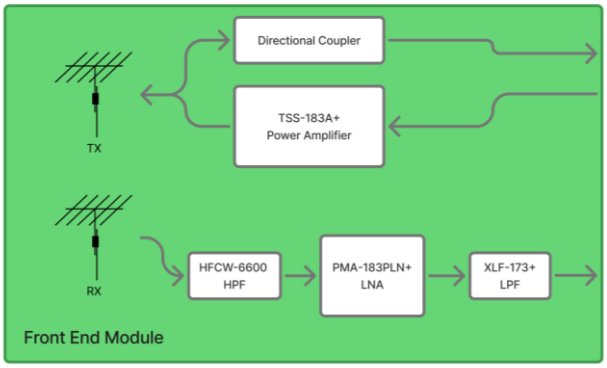


Fig. 3. Front-end module block diagram.

B. Transmitted Waveform Model

The transmitted signal is an FMCW chirp. Its starting phase or code sequence comes from a deterministic seed derived from AWGN samples, and the carrier follows a preset hopping schedule [1], [6], [7]. For transmit channel *m* we write



International Journal of Advanced Research in Computer and Communication Engineering
Impact Factor 8.471 ⁜ Peer-reviewed & Refereed journal ⁜ Vol. 15, Issue 11, November 2026
DOI: 10.17148/IJARCCE.2026.1511139

$$x_m(t) = A_m(t)\exp\left\{j\left[2\pi\int_0^t f_m(\tau)d\tau + \varphi_m\right]\right\} \qquad (1)$$

where $A_m(t)$ is the amplitude envelope, $f_m(t)$ is the instantaneous frequency deviation inside the active hop, and φ_m is the channel-dependent coding phase. The signal at receive channel n is

$$r_n(t) = \sum_{m=1}^{4} \alpha_{mn} x_m(t - \tau_{mn})\exp(j2\pi f_D t) + w_n(t) \qquad (2)$$

where α_{mn} is the combined propagation and channel gain, τ_{mn} is the delay, f_D is the Doppler frequency and $w_n(t)$ is receiver noise.

For the four transmit waveforms to be separable, their cross-correlation must stay low over the relevant delay and Doppler range. The code design and the hop schedule therefore have to be designed together and then verified [1], [8]. Range processing extracts delay, Doppler processing extracts the motion-induced shift, and spatial processing combines the calibrated channels to estimate direction [1], [2], [8].

C. *Range and Aperture*

For a chirp with swept bandwidth B, the ideal range resolution is

$$\Delta R = \frac{c}{2B} \qquad (3)$$

where c is the speed of light. Hopping improves the effective resolution only if the sub-band measurements combine coherently and phase errors stay controlled [7], [9]. The 4TX×4RX array gives up to 16 transmit–receive pairs for virtual-aperture processing, limited by antenna geometry, waveform separation and channel calibration [1], [2], [10].

D. *Design Targets*

The RF operating range is 8–16 GHz. The ADAR1000 gives analog phase control over a nominal 360° in steps of about 2.8°, and amplitude control above 31 dB. These are component specifications, not measured radar performance.

The AD9363 units run in 2×2 IF mode. The usable instantaneous bandwidth, sampling setup, hop timing and coherent stitching still have to be verified against the built SDR and conversion chain [11], [12].

IV. IMPLEMENTATION PLAN

A. *SDR Signal Interface*

The two AD9363 boards generate the transmit signals and capture the receive channels. The software has to set the chirp parameters, the AWGN seed or code sequence, the hop table, the transmit channel assignment, the sampling configuration and the timing alignment. Before the full RF chain is connected, the transmit and receive paths will be checked with loopback and known test signals to measure amplitude, frequency and timing behavior [11], [12].

B. *Reference and Frequency Generation*

An ADF4372 PLL/VCO produces the local-oscillator signals for the conversion chain. Coherent multi-channel processing needs one stable shared reference and controlled signal routing [9]. An ADRF5020 SPDT switch routes the RF/LO paths, and a Wilkinson splitter divides signals across branches with balanced phase and amplitude. LO level, settling time, isolation, hop-switching behavior and phase repeatability will be checked at each output.

C. *IF/RF Conversion and Gain Stages*

The schematic places an HMC694 variable-gain amplifier and a Wilkinson splitter in the main distribution path, with ADRF6780 up-converters, HMC773ALC3B mixers and AVA-183P+ gain blocks in the conversion and conditioning paths. These stages translate frequency, set signal level and route signals between the SDR IF ports and the high-frequency front end. Their presence in the schematic does not confirm conversion gain, noise figure or spurious-free dynamic range, and the conversion plan has to be checked against the exact component variants.

D. *Analog Beamforming Network*

The ADAR1000 devices are set up as separate transmit-only and receive-only modules, so phase and amplitude can be controlled independently at every array element. ADGM1144 SP4T switches add path routing, and AVA-183P+ stages set the intermediate signal levels. Phase and amplitude calibration is needed for each channel and each operating frequency, because board routing differences, component tolerances and frequency-dependent phase can cause beam-steering errors [9], [10], [13].

 This work is licensed under a Creative Commons Attribution 4.0 International License



International Journal of Advanced Research in Computer and Communication Engineering
Impact Factor 8.471 ⁜ Peer-reviewed & Refereed journal ⁜ Vol. 15, Issue 11, November 2026
DOI: 10.17148/IJARCCE.2026.1511139

E. RF Front-End Module

On transmit, the signal passes through a TSS-183A+ power amplifier before the antenna, and a directional coupler takes a sample for power monitoring and possible recalibration [17]. On receive, the signal goes through an HFCW-6600 high-pass filter, a PMA-183PLN+ low-noise amplifier and an XLF-173+ low-pass filter. The filters remove low-frequency and out-of-band harmonic content, and the amplifier raises the signal level before frequency conversion [16]. Isolation, grounding, impedance matching and layout have to keep transmit leakage from desensitizing the receiver [9], [14], [15].

F. Design Tools and Layout

Antenna fields are simulated in CST Studio Suite, the directional coupler is designed in AWR Microwave Office, and the antenna front end and RF distribution board are laid out in Altium Designer. The layout needs wideband impedance matching and deliberate microstrip and grounded-coplanar-waveguide transitions to limit reflections and parasitic coupling. Where possible it should also use equal RF line lengths, continuous ground planes, dense via stitching and physical separation of transmit and receive circuits, to protect phase stability and dynamic range [9], [14], [15].

G. Integration and Test Sequence

Testing proceeds in four steps. First, the antenna and front-end assembly are characterized for impedance match, gain, noise (where measurable) and radiation pattern. Second, the front ends are connected to the distribution network, and the LO, switching, power division, conversion, variable gain and amplification are checked with calibrated narrowband test signals. Third, the SDR interfaces are added, and IF loopback, inter-channel synchronization, gain uniformity and frequency translation are confirmed for both transmit and receive. Fourth, the hopping schedule and coding are enabled, transmit and receive channels are calibrated, and range–Doppler resolution and beam steering are tested with reference targets and recorded data [9]–[12].

V. RESULTS AND DISCUSSION

A. Antenna Simulation

The array was simulated in CST Studio Suite. It uses a compact, symmetric layout of tapered radiating elements, similar in spirit to the antipodal Vivaldi designs in [14], [15], chosen for wideband operation and array processing. Table II lists the observations.

TABLE II. ANTENNA SIMULATION OBSERVATIONS

Item	Observation	Reading
S11	Below −10 dB around the resonant regions	$\|\Gamma\| < 0.32$, under 10 % reflected power
VSWR	Close to the acceptable region over much of X band	Consistent with S11 (−10 dB ↔ VSWR ≈ 1.9)
S21	Coupling between ports across the band	Level still to be read from the plot

Surface current concentrates in the tapered sections, which is the expected excitation. The far-field pattern at 10 GHz has a clear directional main lobe with controlled sidelobes, as a beam-steering array needs. The VSWR and S11 observations agree with each other: S11 = −10 dB corresponds to $|\Gamma| \approx 0.32$, a VSWR of about 1.9 and roughly 10 % reflected power. The S21 curve shows coupling between the antenna ports across the band[14], [15].

Two limits apply. Gain, beamwidth and sidelobe level have not yet been read off the pattern as numbers, so we make no quantitative claim about them. The coupling level in S21 also has to be extracted before we can say how much mutual coupling the array will see. These plots cover the antenna only. They say nothing about the RF distribution network, SDR timing alignment, the AWGN seed coding, the hopping sequence or 4×4 radar processing.

B. Design Values from the Specifications

Table III collects the numbers that follow directly from the component specifications and the architecture. They are design values, not measurements.

 This work is licensed under a Creative Commons Attribution 4.0 International License



International Journal of Advanced Research in Computer and Communication Engineering
Impact Factor 8.471 ⁜ Peer-reviewed & Refereed journal ⁜ Vol. 15, Issue 11, November 2026
DOI: 10.17148/IJARCCE.2026.1511139

TABLE III. DESIGN-LEVEL PARAMETERS

Parameter	Value	Basis
RF range	8–16 GHz (8 GHz span)	Beamformer and front-end limits
Channels	4 TX and 4 RX	2 boards × 2×2 mode
TX–RX pairs	Up to 16	4 × 4 MIMO
Phase control	360°, ≈ 2.8° steps (≈ 128 states)	ADAR1000
Amplitude control	> 31 dB	ADAR1000
Range resolution bound	1.9 cm for B = 8 GHz	Eq. (3); needs full coherent stitching

The range resolution bound needs care. $\Delta R = 1.9$ cm for B = 8 GHz assumes the whole 8–16 GHz span is combined coherently across hops. A single hop is limited by the instantaneous bandwidth of the SDR, so the resolution actually reached will lie between the single-hop value and this bound, depending on how well the hops stitch together [7], [9].

C. Verification Status and Planned Evaluation

Table IV shows where each part of the project stands.

TABLE IV. VERIFICATION STATUS

Item	Status
Antenna array	Simulated; not measured
RF distribution board	Architecture and schematic defined; not measured
SDR boards	Block diagram defined; loopback test pending
ADAR1000 beamforming	Specified; calibration pending
Front-end chain	Schematic defined; gain and noise not measured
Seed-coded hopping waveform	Defined mathematically; not tested
Radar-level metrics	Not yet measured

None of the radar-level metrics has been measured: range resolution, maximum range, detection and false-alarm probability, Doppler accuracy, angle error, post-beamforming sidelobe level, low-probability-of-intercept performance and hop-transition time. They need the assembled hardware and a stated test setup that fixes the chirp bandwidth, hop-sequence length, sampling rate, target range and velocity, signal-to-noise ratio and calibration state. The evaluation should compare a conventional FMCW chirp with the AWGN seed-coded FH-FMCW waveform under identical propagation and target conditions, and each result should be labelled as measured or simulated, never inferred from antenna performance [1], [5]–[9].

VI. CONCLUSION AND FUTURE WORK

This paper surveyed the literature behind an AWGN seed-coded FH-FMCW radar with a 4×4 MIMO array and described the planned architecture. The surveyed work shows that noise-like and phase-coded waveforms can reduce predictability [1], [4]–[6], that MIMO code separation is sensitive to Doppler [8], and that phase noise and channel mismatch limit coherent processing [9], [10]. These points are usually treated separately, and this project aims to combine them on one SDR-based platform.

The architecture uses two AD9363 boards for four transmit and four receive channels, an ADF4372-based reference and LO chain, an RF distribution board, ADAR1000 beamformers and a front end with power amplifier, coupler, filters and low-noise amplifier. Antenna simulation at 10 GHz gives a directional main lobe and S11 below −10 dB near resonance. That supports the antenna choice, but it is antenna-level evidence only, not radar validation.

The next steps are SDR loopback tests, characterization of the LO and hop switching, per-channel calibration, and then range–Doppler and beam-steering tests against a conventional FMCW baseline.

 This work is licensed under a Creative Commons Attribution 4.0 International License



International Journal of Advanced Research in Computer and Communication Engineering
Impact Factor 8.471 ⁜ Peer-reviewed & Refereed journal ⁜ Vol. 15, Issue 11, November 2026
DOI: 10.17148/IJARCCE.2026.1511139

ACKNOWLEDGMENT

The authors thank the Principal, Dr. Nagashettappa Biradar, and the Head of the Department of Electronics and Communication Engineering for their support. We also thank our project guides, Dr. M. Madhumathy and Dr. Venu Gopal B. T., for technical guidance, and the department staff for laboratory access and facilities.

REFERENCES

[1] U. Kumbul, N. Petrov, C. S. Vaucher, and A. Yarovoy, "Phase-coded FMCW for coherent MIMO radar," *IEEE Trans. Microw. Theory Techn.*, vol. 71, no. 6, pp. 2721–2733, Jun. 2023, doi: 10.1109/TMTT.2022.3228950.

[2] H. Park, C. Park, S. Kwak, and S. Lee, "MIMO FMCW radar-based indoor mapping through exploiting multipath signals," *IEEE Internet Things J.*, vol. 11, no. 19, pp. 31479–31491, Oct. 2024, doi: 10.1109/JIOT.2024.3417957.

[3] F. Uysal, "Phase-coded FMCW automotive radar: System design and interference mitigation," *IEEE Trans. Veh. Technol.*, vol. 69, no. 1, pp. 270–281, Jan. 2020, doi: 10.1109/TVT.2019.2953305.

[4] U. Kumbul, N. Petrov, C. S. Vaucher, and A. Yarovoy, "Smoothed phase-coded FMCW: Waveform properties and transceiver architecture," *IEEE Trans. Aerosp. Electron. Syst.*, vol. 59, no. 2, pp. 1720–1737, Apr. 2023, doi: 10.1109/TAES.2022.3206173.

[5] M. A. Govoni, H. Li, and J. A. Kosinski, "Range-Doppler resolution of the linear-FM noise radar waveform," *IEEE Trans. Aerosp. Electron. Syst.*, vol. 49, no. 1, pp. 658–664, Jan. 2013.

[6] G. Galati, G. Pavan, and C. Wasserzier, "Signal design and processing for noise radar," *EURASIP J. Adv. Signal Process.*, vol. 2022, no. 1, Jun. 2022, doi: 10.1186/s13634-022-00884-1.

[7] Y. Zhang *et al.*, "Analysis and simulation of the effect of band hopping jamming on frequency hopping communication system with Simulink," in *Proc. 2022 Int. Conf. Inf. Technol., Commun. Ecosyst. Manag. (ITCEM)*, Bangkok, Thailand, 2022, pp. 174–179, doi: 10.1109/ITCEM57303.2022.00042.

[8] J. Overdevest, F. Jansen, F. Uysal, and A. Yarovoy, "Doppler influence on waveform orthogonality in 79 GHz MIMO phase-coded automotive radar," *IEEE Trans. Veh. Technol.*, vol. 69, no. 1, pp. 16–25, Jan. 2020, doi: 10.1109/TVT.2019.2951632.

[9] P. Tschapek, G. Körner, C. Carlowitz, and M. Vossiek, "Detailed analysis and modeling of phase noise and systematic phase distortions in FMCW radar systems," *IEEE J. Microw.*, vol. 2, no. 4, pp. 648–659, Oct. 2022, doi: 10.1109/JMW.2022.3195574.

[10] P. Yang, G. Chen, and K. Mouthaan, "A dual-polarized 4×4 L-band digital beamforming receiving array with synchronized RFSoCs," in *Proc. 2024 IEEE Asia-Pacific Microw. Conf. (APMC)*, Bali, Indonesia, 2024, pp. 378–380, doi: 10.1109/APMC60911.2024.10867535.

[11] M. Petri and M. Ehrig, "A SoC-based SDR platform for ultra-high data rate broadband communication, radar and localization systems," in *Proc. 2019 Wireless Days (WD)*, Manchester, U.K., 2019, pp. 1–4, doi: 10.1109/WD.2019.8734240.

[12] V. Grigoriev, A. Komissarov, K. Ryutin, and G. Fokin, "Software-defined radio wireless communication technology design. LibreSDR board validation," in *Proc. 2024 Systems of Signals Generating and Processing in the Field of on Board Communications*, Moscow, Russia, 2024, pp. 1–6, doi: 10.1109/IEEECONF60226.2024.10496728.

[13] C. Yan, Z. Zhan, H. Song, and S. Hu, "Design of a highly integrated multifunctional microwave digital composite board for active phased array antenna," in *Proc. 2020 IEEE 5th Int. Conf. Integr. Circuits Microsyst. (ICICM)*, Nanjing, China, 2020, pp. 10–13, doi: 10.1109/ICICM50929.2020.9292205.

[14] T. Fujimoto, M. Sugimoto, and C.-E. Guan, "Improvement of gain in compact antipodal Vivaldi antenna," in *Proc. 2022 IEEE-APS Topical Conf. Antennas Propag. Wireless Commun. (APWC)*, Cape Town, South Africa, 2022, doi: 10.1109/APWC49427.2022.9900025.

[15] K. Kakaraparty and O. Toker, "Multiband antipodal Vivaldi antenna for non-contact radar sensing applications," in *Proc. 2025 Int. Appl. Comput. Electromagn. Soc. Symp. (ACES)*, Orlando, FL, USA, 2025, pp. 1–2, doi: 10.23919/ACES66556.2025.11052586.

[16] M. Sans *et al.*, "Compact wideband balanced bandpass filters with very broad common-mode and differential-mode stopbands," *IEEE Trans. Microw. Theory Techn.*, vol. 66, no. 2, pp. 737–750, Feb. 2018, doi: 10.1109/TMTT.2017.2785246.

[17] N. Hu *et al.*, "Research on high directional waveguide directional coupler," in *Proc. 2019 Int. Conf. Microw. Millim. Wave Technol. (ICMMT)*, Guangzhou, China, 2019, pp. 1–3, doi: 10.1109/ICMMT45702.2019.8992547.

 This work is licensed under a Creative Commons Attribution 4.0 International License